SAND2012-2571C

Damping Models for Shear Beams with Applications to Spacecraft Wiring Harnesses

Jeffrey L. Kauffman* and George A. Lesieutre†
The Pennsylvania State University, University Park, Pennsylvania, 16802, USA
and
Vít Babuška‡
Sandia National Laboratories, Albuquerque, New Mexico, 87185, USA

Spacecraft wiring harnesses can fundamentally alter a spacecraft's structural dynamics, necessitating a model to predict the coupled dynamic response of the structure and attached cabling. While a beam model including first-order transverse shear can accurately predict vibration resonance frequencies, current time-domain damping models are inadequate. For example, the common proportional damping model results in modal damping that depends unrealistically on the frequency. Inspired by a geometric rotation-based viscous damping model that provides frequency-independent modal damping in an Euler-Bernoulli formulation, a time-domain viscous damping model with terms associated with the shear and bending angles is presented. This model demonstrates a much weaker dependence on frequency than proportional damping models. Specifically, the model provides modal damping that is approximately constant in the bending-dominated regime (low mode numbers), increasing by at most 6% for a particular selection of bending and shear angle-based damping coefficients. In the shear-dominated regime (high mode numbers), damping values increase linearly with mode number and are proportional to the shear angle-based damping coefficient. A key feature of this model is its ready implementation in a finite element analysis, requiring only the typical mass, stiffness, and geometric stiffness (associated with axial loads) matrices as developed for an Euler-Bernoulli beam. Such an analysis using empirically determined damping coefficients generates damping values that agree well with existing spacecraft cable bundle data.

Nomenclature

α	viscous damping coefficient
β	shear angle
ϵ	nondimensional shear parameter, $\frac{EI\pi^2}{\kappa AGL^2}$
κ	shear coefficient
$[M]$, $[K]$, and $[K_G]$	beam finite element mass, stiffness, and geometric stiffness matrices
ω_m	natural frequency of vibration
ρ	density
φ	rotation of beam centerline associated with bending
ζ_m	modal damping ratio
A	cross-sectional area
a_m	modal coordinate
E	Young's modulus
G	shear modulus
I	moment of inertia

*Ph.D. Candidate, Department of Aerospace Engineering, 229 Hammond Building, AIAA Student Member.
†Professor and Head, Department of Aerospace Engineering, 229 Hammond Building, AIAA Fellow.
‡Principal Member of the Technical Staff, P.O. Box 5800 MS 0847, AIAA Associate Fellow.

L	length
m	mode number
M_v	internal bending moment
q	distributed lateral load
t	time
V_v	shear force
w	transverse deflection
x	spatial coordinate along beam neutral axis

I. Introduction

Spacecraft contain a large amount of cabling to handle high data and power requirements. With the decreasing density of structural materials and increasing required observation, control, and data transfer capabilities, cables can account for up to 30% of the mass of the spacecraft.[1,2] These cables must be attached to the structure at numerous tiedown points, leading to interaction with and alteration of the spacecraft structure dynamics. Figure 1 shows a typical number of cables with tiedowns in a U.S. Air Force Research Laboratory (AFRL) spacecraft during final integration.

For many spacecraft, the coupled structural dynamics are not initially modeled and are observed through ground system-level testing.[2] While such testing could provide the knowledge required to understand the coupling, it is more desirable and effective to begin with an accurate dynamics model. Furthermore, it may not even be possible to ground test some future deployable spacecraft, meaning an accurate model will be essential, for example, for the design of the spacecraft structural control system.

Previous work modeled the wiring cables and harnesses as beams with effective properties to account for the various materials used in the cabling, insulation, wrapping, and harnessing structures.[1,2,3,4] In addition to the typical mass and stiffness terms, these models incorporated transverse shear effects and employed structural damping through a loss factor in a NASTRAN finite element model. While this approach provided satisfactory results, a better understanding of the physical damping mechanism is preferred for incorporation in a time-domain beam model that accurately represents the cable behavior and the influence the wiring harnesses have on the spacecraft structure.

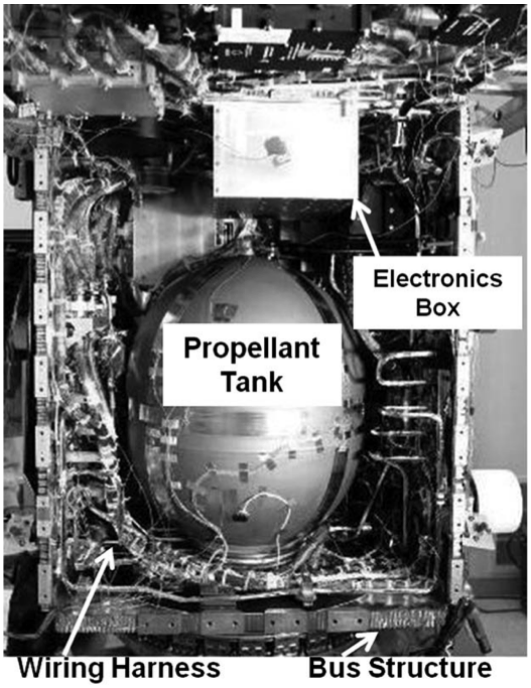

Figure 1. AFRL spacecraft bus with many wrapped and harnessed cable bundles.

II. Damping Model Background

In considering damping models for use with shear beams, it is helpful to look at the variety of damping approaches in Timoshenko beam theory since many will directly translate to shear beam theory upon neglecting any rotary inertia terms. One common approach is a structural damping model involving complex forms of the system parameters. Often incorporated as strain- and shear-based damping mechanisms through the Young's and shear moduli, this method can also include other dissipative mechanisms.[5,6,7,8,9] For example, Lundén and Åkesson considered a complex form for every term in the coupled Timoshenko beam equations, resulting in 14 damping terms, although with the understanding that only a few terms would be non-zero in almost all cases.[7] The boundary conditions can also be included, for example through complex end support and end fixity terms as described by MacBain and Green.[5]

Another common approach to modeling damping in Timoshenko beams is through some variation of proportional viscous damping, often used for its mathematical convenience. In this case, damping terms are a linear combination of the mass and stiffness differential operators, although it is quite common to use only the mass or stiffness operator.[10] For example, some researchers only consider damping associated

with the mass operator with no spatial derivatives – i.e., deflection or rotation alone.[11,12,13,14] Others consider only strain- or shear-based damping, perhaps through a viscoelastic formulation of the constitutive equations.[15,16,17] As with structural damping, the concept of proportional damping can be extended to apply to the boundary conditions to model their associated dissipative mechanisms.[14,18]

Unfortunately, proportional damping is typically unrealistic, providing modal damping that is highly frequency-dependent. With an Euler-Bernoulli beam, using a stiffness-based (mass-based) term only, the damping will increase (decrease) proportionally with the square of the mode number. While this effect is weakened with the inclusion of shear effects, these models will typically provide realistic modal damping values for at most a few modes of vibration within a specific frequency range of interest. Lesieutre addressed this unrealistic behavior, proposing a geometric rotation-based viscous damping model that yields frequency-independent modal damping.[19] An interpretation of this model involves an internal shear force proportional to the time rate of change of the beam slope, and thus a dynamic component of the shear force. One could instead view the term as involving an internal moment proportional to the transverse velocity.

Chen and Russell earlier provided a mathematical treatment of a general approach to frequency-independent modal damping.[20] Representing the second-order governing equation of motion in terms of a spatial differential operator corresponding to strain energy (stiffness), they introduced an additional spatial differential operator to correspond to energy dissipation (damping) that resulted in modal damping that was constant across all modes. Although this approach does not provide any physical interpretation of the damping mechanism, it does present a mathematical model that may be employed when frequency-independent modal damping is desired.

Section III presents the governing equations of motion for a beam with first-order transverse shear effects. The effects of a proposed rotation-based viscous damping model (similar to that developed by Lesieutre for Euler-Bernoulli beams) are demonstrated and compared to those of motion- and strain-based viscous damping models.[19] The models are analyzed using simply-supported boundary conditions to illustrate general trends and provide key insight into damping behavior. Section IV presents a finite element formulation of the proposed model and examines damping behavior using both simply-supported and clamped-clamped boundary conditions. Finally, finite element predictions of damping values for clamped-clamped boundary conditions are compared to those of spacecraft cables tested by Babuška et al. and Goodding et al.[2,3]

III. Governing Equations of Motion

A primary goal of this work is to develop a time-domain damping model that accurately reflects the dynamics of spacecraft power and data cabling. Existing experimental data indicates a shear beam formulation with a damping model that provides approximately frequency-independent modal damping will be especially useful.[3] While an understanding of the corresponding physical mechanism of dissipation is ideal, the mathematical implications of a prospective model are of primary concern. As such, two common viscous damping models (motion-based and strain-based) are analyzed and compared to a proposed model (rotation-based) that is mathematically similar to the rotation-based model proposed by Lesieutre.[19]

III.A. Shear Beam Equations

Consider the governing differential equations for a shear beam (first-order shear term in addition to Euler-Bernoulli formulation; alternatively, a Timoshenko formulation without rotary inertia) without damping. In this case, three variables describe the bending and shear deformation of the beam; however, only two are independent:[21]

$$\beta = \frac{\partial w}{\partial x} - \varphi \tag{1}$$

Using the transverse deflection and the rotation associated with bending, the equations of motion are

$$\begin{aligned} -\frac{\partial}{\partial t}\left(\rho A \frac{\partial w}{\partial t}\right) + \frac{\partial}{\partial x}\left[\kappa A G\left(\frac{\partial w}{\partial x} - \varphi\right)\right] &= -q \\ \frac{\partial}{\partial x}\left(EI\frac{\partial \varphi}{\partial x}\right) + \kappa A G\left(\frac{\partial w}{\partial x} - \varphi\right) &= 0 \end{aligned} \tag{2}$$

For convenience, consider a simply-supported beam with linear, isotropic, homogeneous material and constant cross-section. Representing spatial partial derivatives as $(\,)'$ and temporal partial derivatives as $\dot{(\,)}$,

the coupled equations are then

$$\begin{aligned} -\rho A\ddot{w} + \kappa AG\left(w'' - \varphi'\right) &= -q \\ EI\varphi'' + \kappa AG\left(w' - \varphi\right) &= 0 \end{aligned} \tag{3}$$

For this specialized case of constant parameters, the equations of motion can be rewritten in terms of only one of the three variables. Each of the three possible equations then takes on the same differential form (that is, disregarding the forcing terms):

$$\rho A\ddot{w} - \frac{\rho AEI}{\kappa AG}\ddot{w}'' + EIw'''' = q - \frac{EI}{\kappa AG}q'' \tag{4}$$

$$\rho A\ddot{\varphi} - \frac{\rho AEI}{\kappa AG}\ddot{\varphi}'' + EI\varphi'''' = q' \tag{5}$$

$$\rho A\ddot{\beta} - \frac{\rho AEI}{\kappa AG}\ddot{\beta}'' + EI\beta'''' = -\frac{EI}{\kappa AG}q''' \tag{6}$$

As such, this analysis proceeds in terms of the transverse displacement w; a similar analysis in terms of φ or β produces similar results. With a simply-supported shear beam, the boundary conditions are

$$w(0,t) = w(L,t) = w''(0,t) = w''(L,t) = 0 \tag{7}$$

which result in mode shapes with an integer number of half-sine waves upon solving the associated boundary-value eigenvalue problem:[10]

$$w_m = a_m \sin\frac{m\pi x}{L} \tag{8}$$

Substituting the mode shape into the Equation (4) with zero forcing and neglecting damping yields the unforced, undamped modal equation of motion:

$$\rho A\left[1 + \frac{EI}{\kappa AG}\left(\frac{m\pi}{L}\right)^2\right]\ddot{a}_m + EI\left(\frac{m\pi}{L}\right)^4 a_m = 0 \tag{9}$$

Introducing a nondimensional shear parameter $\epsilon \equiv \frac{EI\pi^2}{\kappa AGL^2}$, the natural frequency is

$$\omega_m = \underbrace{\sqrt{\frac{EI}{\rho A}}\left(\frac{m\pi}{L}\right)^2}_{\text{Euler-Bernoulli}} \frac{1}{\sqrt{1+\epsilon m^2}} \tag{10}$$

The inclusion of transverse shear thus adds a term that reduces the natural frequency from that of an Euler-Bernoulli beam, with the effect greater at higher mode numbers (frequencies). The shear parameter ϵ indicates the influence of transverse shear: as $\epsilon \to 0$, the shear stiffness becomes much greater than the bending stiffness, meaning the beam deflection contains bending only (and the natural frequency of Equation (10) reduces to that of an Euler-Bernoulli beam). For $\epsilon \to \infty$, the bending stiffness is much greater, allowing the beam to only deform in shear. In a similar manner, higher modes can be considered to be shear-dominated with lower modes bending-dominated, as indicated in Figure 2. Certainly a transition between these two regimes exists; a consideration of the shear-based term $\sqrt{1+\epsilon m^2}$ in Equation (10) indicates the point where $\epsilon m^2 = 1$ may be of interest. As such, this transition will be considered to approximately occur at $m = 1/\sqrt{\epsilon}$ (shown in Figure 2 at $m = 10$ for the case of $\epsilon = 0.01$), although in reality the transition occurs over a range of modes.

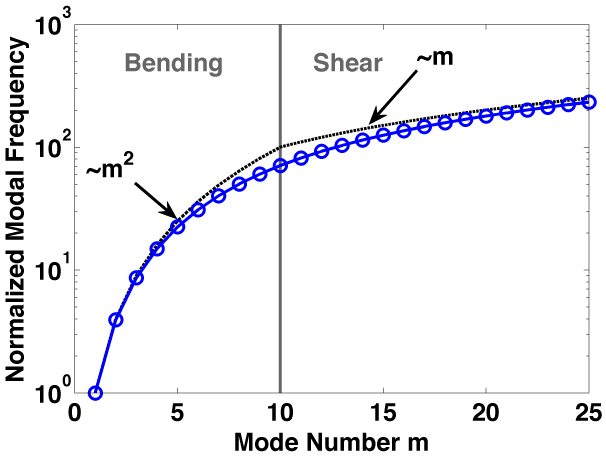

Figure 2. Normalized natural frequency ω_m/ω_1 (blue circles) with asymptotic lines (black dashed lines) for $\epsilon = 0.01$.

III.B. Motion- and Strain-Based Viscous Damping Models

Consider two common damping models that provide proportional damping: motion- and strain-based viscous damping. These models are discussed only for their prevalence in damping modeling and not for any accuracy in describing the nature of the energy dissipation. The motion-based model involves an external lateral force distribution related to and opposing the beam velocity:

$$q = -\alpha_M \dot{w} \tag{11}$$

Strain-based viscous damping involves an internal moment related to the beam centerline curvature rate of change (in time):

$$M_v = \alpha_{EI} \dot{\varphi}' \tag{12}$$

Spatially differentiating the (negative) bending moment twice produces a distributed force for direct incorporation in the governing equations of motion; adding this and the distributed force in Equation (11) to Equation (3) results in the damped governing equations of motion:

$$\begin{aligned} -\rho A \ddot{w} + \kappa AG\left(-\varphi' + w''\right) &= -q + \alpha_M \dot{w} + \alpha_{EI} \dot{\varphi}''' \\ \kappa AG\left(-\varphi + w'\right) + EI\varphi'' &= 0 \end{aligned} \tag{13}$$

Again writing the equations as a single differential equation in w,

$$\rho A \ddot{w} - \frac{\rho AEI}{\kappa AG} \ddot{w}'' + \alpha_M \left(\dot{w} - \frac{EI}{\kappa AG} \dot{w}'' \right) + \alpha_{EI} \dot{w}'''' + EIw'''' = q - \frac{EI}{\kappa AG} q'' \tag{14}$$

Enforcing simply-supported boundary conditions and considering only unforced motion in mode m, the modal equation of motion is

$$\ddot{a}_m \left[\rho A \left(1 + \epsilon m^2\right)\right] + \dot{a}_m \left[\alpha_M \left(1 + \epsilon m^2\right) + \alpha_{EI} \left(\frac{m\pi}{L}\right)^4\right] + a_m \left[EI \left(\frac{m\pi}{L}\right)^4\right] = 0 \tag{15}$$

Comparing to the unforced canonical equation of motion

$$\ddot{a}_m + 2\zeta_m \omega_m \dot{a}_m + \omega_m^2 a_m = 0 \tag{16}$$

the modal damping is

$$\zeta_m = \frac{1}{2\sqrt{\rho AEI}} \left[\alpha_M \frac{\sqrt{1 + \epsilon m^2}}{\left(\frac{m\pi}{L}\right)^2} + \alpha_{EI} \frac{\left(\frac{m\pi}{L}\right)^2}{\sqrt{1 + \epsilon m^2}} \right] \tag{17}$$

As in the previous analysis, these damping models have different behaviors in the bending- and shear-dominated regimes. Quantifying these effects in terms of Equation (17),

$$\zeta_m \sim \begin{cases} \alpha_M \frac{L^2}{\pi^2} \frac{1}{m^2} + \alpha_{EI} \frac{\pi^2}{L^2} m^2 & \epsilon m^2 \ll 1 \\ \alpha_M \frac{L^2}{\pi^2} \frac{\sqrt{\epsilon}}{m} + \alpha_{EI} \frac{\pi^2}{L^2} \frac{m}{\sqrt{\epsilon}} & \epsilon m^2 \gg 1 \end{cases} \tag{18}$$

Specifically, motion-based (strain-based) viscous damping produces modal damping ratios that decrease (increase) with the square of the mode number in the bending-dominated regime and the mode number in the shear-dominated regime, as shown in blue circles (cyan squares) in Figure 3(a). Noting that the normalized damping values (that is, normalized by the damping of the first vibration mode ζ_m/ζ_1) in Figure 3(a) are plotted on a logarithmic scale, the damping values produced by motion- and strain-based viscous damping models quickly become unrealistic, at least for this application. Typical shear parameter values are $\epsilon \approx 0.01 - 0.03$ for the spacecraft cables tested by Babuška et al.[2] For the particular case of $\epsilon = 0.01$, the strain-based model produces modal damping values that increase thirty-fold over the first six modes; data presented by Goodding et al. show that actual cable damping values change by at most a factor of two.[3]

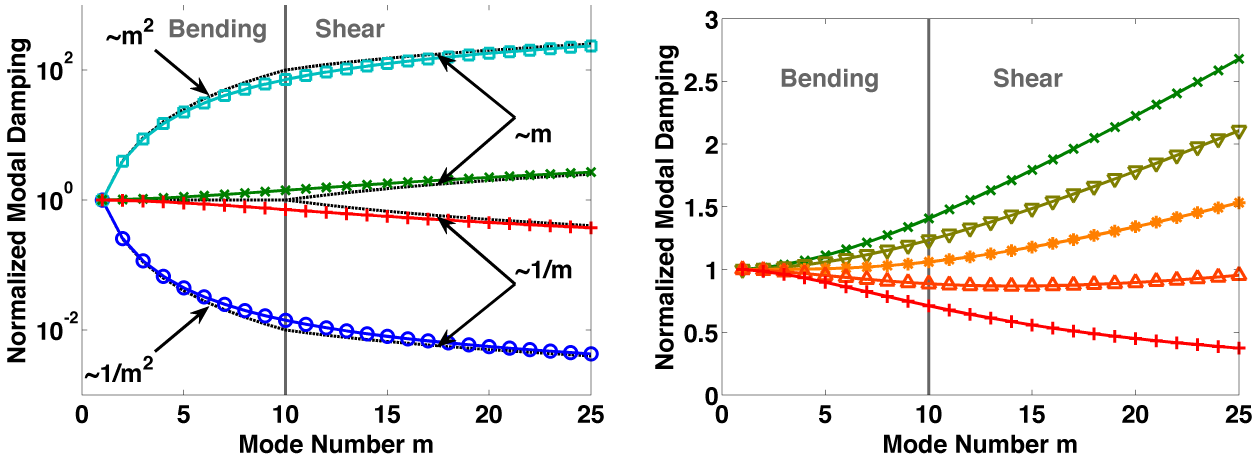

(a) Motion-based (blue circles), strain-based (cyan squares), and rotation-based damping models with $\alpha_\beta/\alpha_\varphi = 0$ (red crosses) and $\alpha_\beta/\alpha_\varphi = 1$ (green x's).

(b) Rotation-based damping models with $\alpha_\beta/\alpha_\varphi = 0$ (red crosses), 1/4 (dark orange up triangles), 1/2 (light orange asterisks), 3/4 (olive down triangles), and 1 (green x's).

Figure 3. Frequency dependence of normalized modal damping for several viscous damping models, with $\epsilon = 0.01$.

III.C. Rotation-Based Viscous Damping Model

Consider now a rotation-based damping model similar to that proposed by Lesieutre.[19] For a shear beam, this model can be viewed as two internal shear forces associated with the time rate of change of the shear and beam centerline bending angles:

$$V_v = -\alpha_\beta \dot{\beta} - \alpha_\varphi \dot{\varphi} \tag{19}$$

This force can of course be described in terms of other variables using Equation (1); however, this particular representation provides perhaps the best physical understanding of the damping mechanism. More significantly, it allows selection of the two damping coefficients to correspond with mechanisms associated with shear and bending deformation. Differentiating the shear force with respect to x and including it in the equation of motion results in

$$\begin{aligned} -\rho A \ddot{w} + \kappa AG\left(-\varphi' + w''\right) &= -q - \alpha_\beta \dot{\beta}' - \alpha_\varphi \dot{\varphi}' \\ \kappa AG\left(-\varphi + w'\right) + EI\varphi'' &= 0 \end{aligned} \tag{20}$$

Once again a single equation of motion can describe the beam dynamics, shown here in terms of the bending rotation φ:

$$\rho A \ddot{\varphi} - \frac{\rho AEI}{\kappa AG}\ddot{\varphi}'' - \alpha_\phi \dot{\varphi}'' + \alpha_\beta \frac{EI}{\kappa AG}\dot{\varphi}'''' + EI\varphi'''' = q' \tag{21}$$

Considering only motion in mode m with simply-supported boundary conditinos, the modal equation of motion is

$$\ddot{a}_m\left[\rho A\left(1+\epsilon m^2\right)\right] + \dot{a}_m\left[\left(\frac{m\pi}{L}\right)^2\left(\alpha_\varphi + \alpha_\beta \epsilon m^2\right)\right] + a_m\left[EI\left(\frac{m\pi}{L}\right)^4\right] = 0 \tag{22}$$

Comparing to the unforced canonical equation of motion, the modal damping is

$$\zeta_m = \frac{1}{2\sqrt{\rho AEI}} \frac{\alpha_\varphi + \alpha_\beta \epsilon m^2}{\sqrt{1+\epsilon m^2}} \tag{23}$$

Figure 3(a) also shows these damping values for $\alpha_\beta = 0$ (red crosses) and $\alpha_\beta = \alpha_\varphi$ (green x's), clearly displaying how this model provides modal damping with significantly greater frequency-independence that the motion- and strain-based models. Furthermore, a wide range of damping curves can be produced by proper selection of the damping coefficients. Figure 3(b) demonstrates this range, showing the normalized modal damping (ζ_m/ζ_1) for several selections of $\alpha_\beta/\alpha_\varphi$.

A key feature of this model and this representation in particular is the separation of shear- and bending-related damping contributions. Recalling that lower modes of vibration are bending-dominated and higher

modes are shear-dominated, it is perhaps unsurprising that the bending-related damping term is most important at low mode numbers and the shear-related term dominates at high mode numbers:

$$\zeta_m \sim \begin{cases} \alpha_\varphi & \epsilon m^2 \ll 1 \\ \alpha_\beta \sqrt{\epsilon} m & \epsilon m^2 \gg 1 \end{cases} \tag{24}$$

Indeed, Figure 3(b) shows little variation in damping over the first few modes regardless of α_β. At higher modes, however, α_β plays a much more significant role, determining the slope of the normalized damping curve.

III.D. Mathematical Form of Frequency-Independent Modal Damping

Based on existing spacecraft power and data cable damping data, it is of interest to develop a viscous damping model that provides frequency-independent modal damping. Consider again the undamped differential forms of Equations (4)-(6). The unforced equation of motion could instead be written in terms of spatial differential operators, for example:[10]

$$\mathcal{M}\ddot{w} + \mathcal{C}\dot{w} + \mathcal{K}w = 0 \tag{25}$$

where

$$\mathcal{M} = \rho A \left(1 - \frac{EI}{\kappa AG}()''\right) \qquad \text{and} \qquad \mathcal{K} = EI()'''' \tag{26}$$

A key departure from the framework presented by Chen and Russell is the inclusion of transverse shear: here the kinetic energy (mass) is also associated with a spatial differential operator.[20] Nonetheless, one can still choose $\mathcal{C}$ to yield a desired level of constant damping ζ_0, independent of frequency:

$$\mathcal{C} = 2\zeta_0\sqrt{\mathcal{K}\mathcal{M}} \tag{27}$$

The square root of $\mathcal{K}$ is rather straight-forward, but $\sqrt{\mathcal{M}}$ does not simplify to a term containing only whole derivatives. Instead, consider a series expansion of the quantity:

$$\sqrt{\mathcal{M}} = \sqrt{1 - \frac{EI}{\kappa AG}()''} \approx 1 - \frac{1}{2}\frac{EI}{\kappa AG}()'' - \frac{1}{8}\left(\frac{EI}{\kappa AG}\right)^2()'''' - \cdots \tag{28}$$

Comparing to Equation (21), the proposed rotation-based viscous damping model with $\alpha_\beta/\alpha_\varphi = 1/2$ is exactly the two-term series expansion of frequency-independent modal damping. In other words, the model provides damping behavior that exhibits the greatest amount of frequency-independence without incorporating higher-order spatial derivatives (at least sixth-order) or fractional derivatives in the equation of motion. Figure 3(b) also demonstrates that selecting $\alpha_\beta/\alpha_\varphi = 1/2$ (curve with asterisks) results in approximately constant modal damping, at least throughout the bending regime. Recalling Equation (23), the modal damping increases approximately 6% from the first mode to the bending- / shear-dominated regime transition ($\epsilon m^2 = 1$). Smaller values of $\alpha_\beta/\alpha_\varphi$ result in an initial decrease of damping values and could extend the range of approximately frequency-independent modal damping (as with $\alpha_\beta/\alpha_\varphi = 1/4$, the curve with up triangles in Figure 3(b)).

IV. Damping Results & Experimental Data

IV.A. Finite Element Formulation

While the special case of simply-supported boundary conditions allows an analytical treatment and provides excellent insight into the behavior of the various damping models, a more general approach is preferred. As such, consider a single equation of motion incorporating the motion-, rotation-, and strain-based viscous damping terms:

$$\rho A\ddot{\varphi} - \frac{\rho AEI}{\kappa AG}\ddot{\varphi}'' + \alpha_M\left(\dot{\varphi} - \frac{EI}{\kappa AG}\dot{\varphi}''\right) - \alpha_\phi\dot{\varphi}'' + \alpha_\beta\frac{EI}{\kappa AG}\dot{\varphi}'''' + \alpha_{EI}\dot{\varphi}'''' + EI\varphi'''' = q' \tag{29}$$

Using the weak form of the equation of motion and integrating by parts leads to a finite element formulation that employs the typical mass $[M]$, stiffness $[K]$, and geometric stiffness $[K_G]$ (related to axial loading)

finite element matrices. Notably, the proposed viscous damping terms can be readily implemented in a finite element formulation using commonly available matrices:

$$\left[\rho A\left([M]+\frac{EI}{\kappa AG}[K_G]\right)\right]\left\{\ddot{a}\right\}+\left[\alpha_M[M]+\left(\alpha_M\frac{EI}{\kappa AG}+\alpha_\varphi\right)[K_G]+\left(\alpha_\beta\frac{EI}{\kappa AG}+\alpha_{EI}\right)[K]\right]\left\{\dot{a}\right\} + \left[EI[K]\right]\left\{a\right\}=\left\{F\right\} \tag{30}$$

Figure 4 shows the results of such an implementation, for both simply-supported (solid lines, SS) and clamped-clamped (dashed lines, CL-CL) boundary conditions. In fact, the analytical results of Equation (23) are also plotted on this graph and coincide with those produced by the finite element analysis, confirming the validity of the modeling approach. The damping behavior of the rotation-based model with clamped-clamped boundary conditions departs significantly from that of simply-supported boundary conditions in the bending-dominated regime. It is reduced approximately 45% in the first mode, increases rapidly with mode number, and then approximately equals that of simply-supported boundary conditions throughout the shear-dominated regime. In general, the damping values of the first few modes are dependent on the boundary conditions; however, boundary conditions have little effect at higher mode numbers. If frequency-independent modal damping were a key goal, a potential modeling approach would be to incorporate some level of motion-based viscous damping – it provides appreciable damping in the first few modes only, decreasing with the square of the mode number. Note that this is purely a mathematical solution, not an indication of the underlying physical explanation for differing damping values.

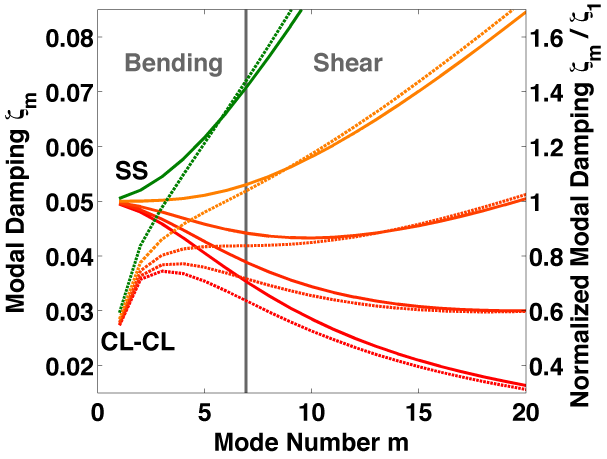

Figure 4. Predicted modal damping values for simply-supported (SS) and clamped-clamped (CL-CL) boundary conditions with $\alpha_\varphi = 0.05$ and $\alpha_\beta/\alpha_\varphi = 0$, 1/10, 1/4, 1/2, and 1 (from bottom to top), with $\epsilon = 0.021$.

IV.B. Model-Data Comparison

With the finite element analysis in agreement with the analytical calculations of damping values, the most significant test of the model's utility is a comparison to experimental data. In this particular application, spacecraft cable bundles are of primary importance. These bundles consist of multiple twisted wire pairs that are stitched together and wrapped in Kapton; this process and the resulting experimental data with corresponding cable parameters are presented extensively by Ardelean et al., Babuška et al., Goodding et al., and Coombs et al.[1,2,3,4] Figure 5(a) displays the modal damping values for over one hundred of these spacecraft cable bundles with clamped-clamped boundary conditions. The data comes from twelve families of bundles, with all bundles within a family having approximately equal properties (ρ, κ, A, G, E, and I). This difference in families at least partially explains the spread in measured damping values in Figure 5(a), where the mean values are plotted as diamonds and the one and two standard deviation range are the dark and light shaded areas. However, even data for a single family contains considerable variation, as shown in Figure 5(b).

In all cases, the nondimensional shear parameter for these cables is $\epsilon < 0.03$, indicating the transition between bending- and shear-dominated regimes occurs at the sixth mode or higher; that is, the data in Figure 5 can largely be considered to reside in the bending-dominated regime. In general, the spacecraft cable bundles exhibit a slight decrease in modal damping values with mode number, perhaps up to 20%. To compare these values to those produced by the finite element analysis, consider a single family of cable bundles so that nominally identical cable bundle properties can be used. Figure 5(b) shows the experimentally measured damping values for thirteen bundles (blue squares), their mean values (black diamonds) and one and two standard deviations (dark and light shaded areas), and the values produced by a finite element analysis (red solid line) with $\alpha_M = 0.043$, $\alpha_\varphi = 0.038$, and $\alpha_\beta/\alpha_\varphi = 0.3$. These damping coefficients are selected empirically to fit best with measured data and could be selected for each cable bundle family.

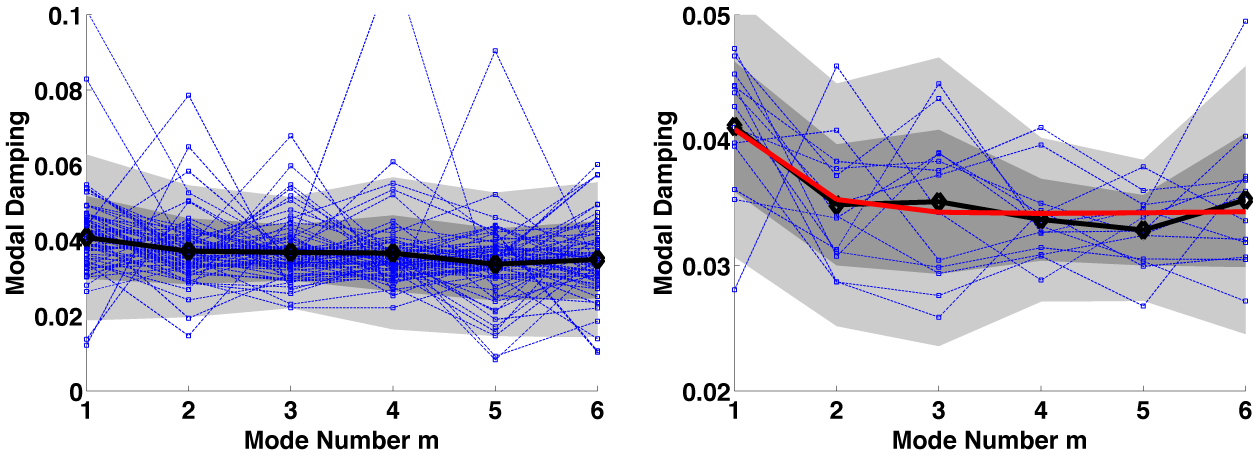

(a) Data for 12 families, each consisting of several cables with nominally identical properties.

(b) Data for one family with finite element damping values using $\alpha_M = 0.043$, $\alpha_\varphi = 0.038$, and $\alpha_\beta/\alpha_\varphi = 0.3$.

Figure 5. Modal damping values from experimental testing of individual cables (blue squares / dashed lines), with mean values (black diamonds / solid lines) and one and two standard deviations (dark and light shaded areas).

V. Conclusions

This research seeks to provide a physically accurate time-domain viscous damping model for a shear beam for use in modeling spacecraft wiring harnesses. Such a model is developed building on a geometric rotation-based model that provides frequency-independent modal damping for an Euler-Bernoulli beam. This model includes two terms associated with the time rate of change of both the beam centerline bending and shear angles. This approach allows selection of two parameters to best represent the damping; the term associated with the bending (shear) angle is the dominant factor in the bending-dominated (shear-dominated) regime. Furthermore, modal damping values are approximately constant (at least for simply-supported boundary conditions) in the bending-dominated regime, increasing by at most 6% when $\alpha_\beta/\alpha_\varphi = 1/2$. A second key feature of this model is that it can be implemented numerically using common Euler-Bernoulli beam finite element matrices. A finite element analysis confirms the analytical results for the case of simply-supported boundary conditions. Clamped-clamped boundary conditions alter this approximate frequency-independence, reducing the modal damping of the first few modes. In this case, including a motion-based viscous damping term increases the modal damping of the first few modes and can restore an approximately frequency-independent behavior. This approach generates good agreement between experimental data and a finite element analysis using empirically determined damping coefficients.

The rotation-based viscous damping model proposed here does provide some physical understanding of the energy dissipation mechanisms; however, it is used primarily for its mathematical convenience. All comparisons with experimental data make use of empirically fit damping coefficients; ideally, these coefficients could be calculated a priori based on beam properties. Additional explanation of the underlying physics of the energy dissipation would aid in these calculations. Finally, it is also of interest to examine and develop viscous damping models with similar characteristics for a Timoshenko beam for those cases when rotary inertia cannot be neglected.

Acknowledgments

This work was supported by Sandia National Laboratories. Sandia National Laboratories is a multi-program laboratory managed and operated by Sandia Corporation, a wholly owned subsidiary of Lockheed Martin Corporation, for the United States Department of Energys National Nuclear Security Administration under contract DE-AC04-94AL85000. The authors also wish to thank Hartono “Anton” Sumali as well as Emil Ardelean, Douglas Coombs, and James Goodding for thoroughly explaining the experimental process and indicating the most useful and robust cable data.

References

[1]Ardelean, E. V., Goodding, J. C., Coombs, D. M., Griffee, J. C., Babuška, V., III, L. M. R., and Lane, S. A., "Cable Effects Study: Tangents, Rat Holes, Dead Ends, and Valuable Results," *Proceedings of the Fifty-First AIAA/ASME/ASCE/AHS/ASC Structures, Structural Dynamics, and Materials Conference*, AIAA 2010-2806, Orlando, FL, 2010.

[2]Babuška, V., Coombs, D. M., Goodding, J. C., Ardelean, E. V., Robertson, L. M., and Lane, S. A., "Modeling and Experimental Validation of Space Structures with Wiring Harnesses," *Journal of Spacecraft and Rockets*, Vol. 47, No. 6, Nov.–Dec. 2010, pp. 1038–1052.

[3]Goodding, J. C., Ardelean, E. V., Babuška, V., Robertson III, L. M., and Lane, S. A., "Experimental Techniques and Structural Parameter Estimation Studies of Spacecraft Cables," *Journal of Spacecraft and Rockets*, Vol. 48, No. 6, Nov.-Dec. 2011, pp. 942–957.

[4]Coombs, D. M., Goodding, J. C., Babuška, V., Ardelean, E. V., Robertson, L. M., and Lane, S. A., "Dynamic Modeling and Experimental Validation of a Cable-Loaded Panel," *Journal of Spacecraft and Rockets*, Vol. 48, No. 6, Nov.-Dec. 2011, pp. 958–973.

[5]MacBain, J. C. and Genin, J., "Energy dissipation of a vibrating Timoshenko beam considering support and material damping," *International Journal of Mechanical Sciences*, Vol. 17, No. 4, April 1975, pp. 255–265.

[6]Irie, T., Yamada, G., and Takahashi, I., "The steady state out-of-plane response of a Timoshenko curved beam with internal damping," *Journal of Sound and Vibration*, Vol. 71, No. 1, July 1980, pp. 145–156.

[7]Lundén, R. and Åkesson, B., "Damped second-order Rayleigh-Timoshenko beam vibration in space – an exact complex dynamic member stiffness matrix," *International Journal for Numerical Methods in Engineering*, Vol. 19, No. 3, March 1983, pp. 431–449.

[8]Chen, Y.-H. and Sheu, J.-T., "Axially-loaded damped Timoshenko beam on viscoelastic foundation," *International Journal for Numerical Methods in Engineering*, Vol. 36, No. 6, March 1993, pp. 1013–1027.

[9]Esmailzadeh, E. and Jalili, N., "Optimum Design of Vibration Absorbers for Structurally Damped Timoshenko Beams," *Journal of Vibration and Acoustics*, Vol. 120, No. 4, Oct. 1998, pp. 833–841.

[10]Meirovitch, L., *Principles and Techniques of Vibrations*, Prentice Hall, Upper Saddle River, NJ, 1997.

[11]Huang, T. C. and Huang, C. C., "Free Vibrations of Viscoelastic Timoshenko Beams," *Journal of Applied Mechanics*, Vol. 38, No. 2, June 1971, pp. 515–521.

[12]Soufyane, A. and Wehbe, A., "Uniform Stabilization for the Timoshenko Beam by a Locally Distributed Damping," *Electronic Journal of Differential Equations*, Vol. 2003, No. 29, March 2003, pp. 1–14.

[13]Muñoz Rivera, J. E. and Racke, R., "Global Stability for Damped Timoshenko Systems," *Discrete and Continuous Dynamical Systems*, Vol. 9, No. 6, Nov. 2003, pp. 1625–1639.

[14]Lee, H.-L. and Chang, W.-J., "Effects of Damping on the Vibration Frequency of Atomic Force Microscope Cantilevers Using the Timoshenko Beam Model," *Japanese Journal of Applied Physics*, Vol. 48, No. 6, June 2009, pp. 065005.

[15]Banks, H. T. and Wang, Y., "Damping Modeling in Timoshenko Beams," *Proceedings of the 1992 American Control Conference*, IEEE, Chicago, IL, June 1992, pp. 2139–2143.

[16]Zhao, H. L., Liu, K. S., and Zhang, C. G., "Stability for the Timoshenko Beam System with Local Kelvin-Voigt Damping," *Acta Mathematica Sinica*, Vol. 21, No. 3, June 2005, pp. 655–666.

[17]Chen, W.-R., "Bending vibration of axially loaded Timoshenko beams with locally distributed Kelvin-Voigt damping," *Journal of Sound and Vibration*, Vol. 330, No. 13, June 2011, pp. 3040–3056.

[18]Xu, G. Q. and Yung, S. P., "Exponential Decay Rate for a Timoshenko Beam with Boundary Damping," *Journal of Optimization Theory and Applications*, Vol. 123, No. 3, Dec. 2004, pp. 669–693.

[19]Lesieutre, G. A., "Frequency-Independent Modal Damping for Flexural Structures via a Viscous "Geometric" Damping Model," *Journal of Guidance, Control, and Dynamics*, Vol. 33, No. 6, Nov.–Dec. 2010, pp. 1931–1935.

[20]Chen, G. and Russell, D. L., "A Mathematical Model for Linear Elastic Systems with Structural Damping," *Quarterly of Applied Mathematics*, Vol. 39, Jan. 1982, pp. 433–454.

[21]Shames, I. H. and Dym, C. L., *Energy and Finite Element Methods in Structural Mechanics*, Taylor & Francis, New York, NY, 2003.